Repulsive Forces and Relaxation on Compression of Entangled, Polydisperse Polystyrene Brushes

Marina Ruths,* Diethelm Johannsmann,* Jürgen Rühe, and Wolfgang Knoll

Max-Planck-Institute for Polymer Research, Ackermannweg 10, D-55128 Mainz, Germany

Received December 14, 1999

ABSTRACT: The interaction forces between high molecular weight polystyrene brushes ($M_n = (0.7-1.2) \times 10^6$ g/mol), formed by radical chain polymerization from an initiator chemically bound to silica (quartz-glass) substrates, were measured with a surface forces apparatus. Because of the high grafting densities obtained (7−10 nm between attachment points), the polymer chains were strongly stretched and extended several hundred nanometers from each surface in a good solvent. The extension and magnitude of the purely repulsive force measured over the whole interaction range were compared to theoretical predictions, taking into account the polydispersity of the polymer. The differences in range and magnitude between forces measured on approach and on separation of the surfaces increased after long compression times and were attributed to entanglements within each compressed layer.

Introduction

In many applications it is essential that adsorbed molecules (surface coatings or lubricants) remain localized at a solid−liquid interface when exposed to different solvents or to external pressure from another surface. For example, to avoid aging effects in suspensions or to promote adhesion, it is often desirable to modify interfaces uniformly and permanently with selectively adsorbed polymer.[1] In experimental studies of friction and boundary lubrication, it has been found that covalently bound lubricant layers are more effective in protecting sliding surfaces against wear than physisorbed molecules that are easily removed from small areas where, as a result, damage occurs first.[2]

It is commonly observed that only a limited layer thickness can be obtained by adsorption of polymer from solution, since after some chains have become attached, incoming chains have to diffuse against a concentration gradient to reach the solid surface. In addition, there is an entropy loss arising from the change in conformation of both the incoming and the adsorbed polymer to accommodate another chain. For these reasons, typically only a few milligrams of polymer per square meter adsorbs onto a solid surface from a good or Θ solvent, regardless of whether the chains become chemically bound to the surface or only physisorbed.[3]

The equilibrium conformation of end-grafted chains arises from a balance between polymer−polymer and polymer−solvent interactions, as for unattached chains. Grafted chains stretch away from the surface in order to reduce their interaction with other chains, attaining a different conformation than the optimal for free chains in bulk or in solution. Different models[4−11] for the segment density profile normal to the surface and the interactions between two opposed surfaces have been developed for different solvent conditions and regions of overlap (stretching), based on this balance between osmotic pressure and elastic restoring force. In order of increasing overlap (decreasing distance between attachment points), the model regions are called pancake, mushroom, and brush layers.[7] The theoretical models have also been extended to polydisperse brushes,[12] but systematic experimental studies of such brushes are rare even though this situation is commonly encountered in applications such as sterically stabilized dispersions.

Interaction forces between two polymer-coated surfaces can be measured in a well-defined geometry with a surface forces apparatus (SFA). The standard substrate in the SFA is muscovite mica, a mineral that can be cleaved to large (several cm^2), atomically smooth sheets. The disadvantage of mica substrates is that they are unreactive. To study surfaces of different structure and composition, mica surfaces have been covered by various physisorbed organic or inorganic layers such as Langmuir−Blodgett or self-assembled surfactant[13,14] or modified lipid layers,[15] end-functionalized polymer[16] or block-copolymer[17−19] layers; or electron-beam or chemical vapor deposited Al_2O_3 or SiO_2.[2,20]

The aim of the present study is (i) to suggest a procedure for preparing robust substrates suitable for chemical grafting, based on the existing technique of replacing the mica surfaces in the SFA with thin, flexible silica (quartz-glass) sheets,[21−24] and (ii) to study the interactions between high molecular weight polymer brushes with grafting densities exceeding the ones obtainable by physisorption of functionalized long chains from solution. We have chosen to study high molecular weight, polydisperse polystyrene brush layers in toluene at 25 °C (good solvent conditions). The brushes were formed by a grafting-from technique,[25−27] by which dry layer thicknesses of more than 100 nm of polystyrene with a molecular weight around 1×10^6 g/mol and a grafting distance between chains as low as 3−4 nm have been obtained on large planar surfaces.[28] In contrast to physisorbed systems, where the distance between grafted, long chains is expected to scale with molecular weight as $M^{0.6}$,[5] different, high grafting densities for high molecular weights could be chosen by varying the polymerization conditions.[25−27]

Methods and Materials

Instrumentation. The interaction forces were measured with a "Mark II" surface forces apparatus (SFA).[29] In this instrument, two transparent, back-silvered surfaces face each other in a crossed-cylinder configuration (equivalent to a

* Authors for correspondence.

10.1021/ma9920994 CCC: $19.00 © 2000 American Chemical Society
Published on Web 04/22/2000

sphere near a flat surface). The separation between the surfaces, D, is measured by multiple beam interferometry,[30,31] as the base of a double cantilever leaf spring supporting the lower surface is moved with respect to the base of the rigidly mounted upper surface by means of motor-driven mechanical stages.

The interaction force, F, is calculated from the deflection of the spring, i.e., the difference in measured separation distance compared to the one expected from a calibration of distance vs motor movement at large separation where no force acts between the surfaces. A strong repulsive force was expected between the polymer layers at small separations (large compression), and a spring constant of 9×10^5 mN/m was chosen to facilitate the measurements, while still retaining sufficient sensitivity to detect the onset of the interactions. On the basis of previous investigations with other techniques,[32−34] these brushes were also expected to extend far from the surfaces in a good solvent. The maximum range of the more sensitive mechanical distance control in our instrument was just over 10 μm. (The range depends on the spring constants of the mechanisms used to reduce the movement of a micrometer-driven shaft.) The measurements of the large extension and repulsive force in our systems required about half of this range and were close to the limit of what was experimentally accessible with our current setup. For this reason, it was advantageous to work on contact positions with as small a radius of curvature as possible ($R \approx 1$ cm). The force measurements are presented as F/R to allow comparison between different experiments and with the energy between flat plates, $W(D) = F(D)/(2\pi R)$.[35]

Silica Surfaces. To study covalently bound systems, we replaced the mica substrates normally used in the SFA with silica (quartz-glass) sheets of comparable thickness. The procedure used was a simplification of the method developed by Horn and co-workers.[21−24] Thin quartz-glass bubbles with a diameter of 5−8 cm were blown from a tube (Suprasil, Heraeus Quarzglas, Germany) sealed at one end in an oxygen−hydrogen flame. The bubbles eventually ruptured during blowing, and flexible, irregularly shaped pieces with an area of 1−2 cm^2 and a thickness of a few micrometers could easily be removed with tweezers from around the wide opening formed.

The silica pieces were immediately placed on a freshly cleaved, thick mica backing sheet. Since they were slightly curved, only their center region (0.4−0.8 cm^2) adhered to the backing sheet. The roughness of the silica could not be discerned at this point, and clean pieces appeared to adhere as well to the backing sheet as mica pieces. It has been shown that the adhesion between such silica pieces and mica, and also between two silica pieces, is of the same order of magnitude as between two mica sheets despite the slightly larger roughness.[21] The edges of the curved pieces were covered with freshly cleaved mica pieces to prevent contamination of the exposed rim of the side facing the backing sheet during the subsequent vapor deposition of silver (55 nm). When the silica pieces were glued with their silvered side down onto half-cylindrical support disks, care was taken to ensure that the part that had adhered to the backing sheet was positioned over the top section.

An atomic force microscopy (AFM) image (Figure 1a) obtained in tapping mode (Nanoscope IIIa, Digital Instruments) of a 5×5 μm^2 area that had previously been in adhesive contact with a mica backing sheet showed an rms roughness of 0.2 nm. The roughness of different silica sheets was in the range 0.2−0.3 nm, also over areas comparable to the contact region in the SFA, 30×30 μm^2, in agreement with the rms roughness of 0.5 nm along a trace of 30 μm obtained from profilometry measurements[21] and AFM measurements giving an upper bound of 0.4 nm over a 12×12 μm^2 area.[23] Some isolated, immobile protrusions were always present on the surfaces (cf. arrows in Figure 1a). The height profile (Figure 1b) along the line indicated in Figure 1a shows one typical such structure with a height of about 2 nm and a diameter of 50 nm. The phase image observed in tapping mode suggested that the material in the protrusions was of similar

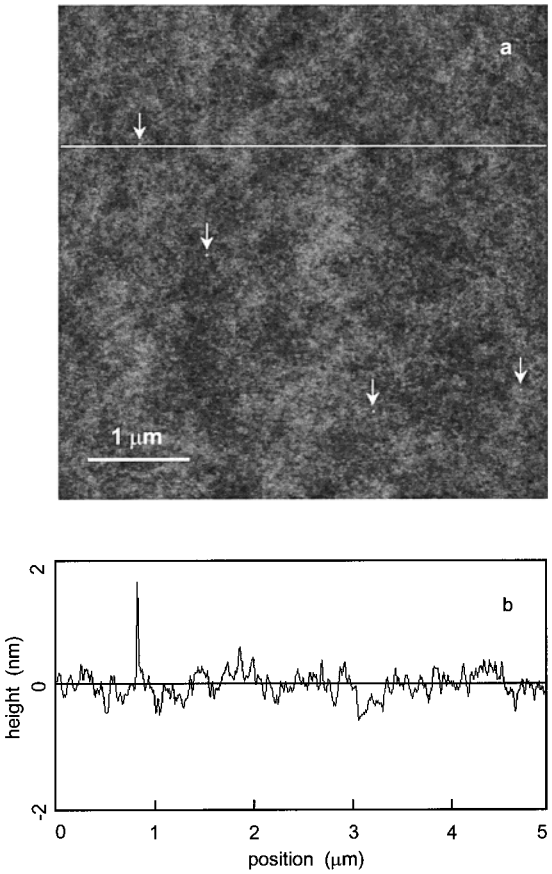

Figure 1. (a) AFM image of a 5×5 μm^2 area of a quartz-glass sheet with an rms roughness of 0.2 nm. The larger protrusions observed are indicated with arrows. (b) Height profile along the line drawn across (a).

stiffness as the surrounding quartz-glass surface, and they may thus also consist of silica. As described above, the presence of a few protrusions did not prevent the bare, clean surfaces from coming into adhesive contact. The consequences of a number of protrusions for measurements of short-range forces are beyond the scope of this study. The effect of the overall roughness on the accuracy of the distance measurements compared to mica substrates will be discussed below.

The advancing contact angle of water on clean, untreated silica sheets was 44−47° and the contact angle of a stationary drop was 30−35° (stable for 5−10 min), which is in good agreement with results reported in refs 23 and 20, respectively. The density of silanol groups on such flamed silica surfaces given in the literature is 1.9×10^{18} m^{-2},[23] which amounts to about 40% of full hydrolyzation.[36] After treatment with an ozone-generating UV Pen-Ray lamp (Oriel, effect 18 W) for 30 min or 1−1.5 h at a distance of 1−1.5 cm, the surface became more hydrophilic with a contact angle of water of ca. 15° or <8° (spreading rapidly), respectively. However, such a modification was not needed to enable binding of the polymerization initiator in our experiment, and the grafting was therefore done on untreated surfaces.

Distance Measurement. The separation distance between the surfaces, D, is measured from the wavelengths of constructively interfering light emerging from the optical cavity formed by the back-silvered substrates and the intervening sample. A calibration based on the contact between the two substrates without sample is necessary to account for their thickness. The procedure of calculating the distance for the case of a symmetrical interferometer (two substrates of equal thickness) is given in ref 30. Since the silica sheets originate from different parts of a bubble, two pieces never have exactly the same thickness, and it also varies across each piece. Two silica sheets in contact thus form an asymmetrical interfer-

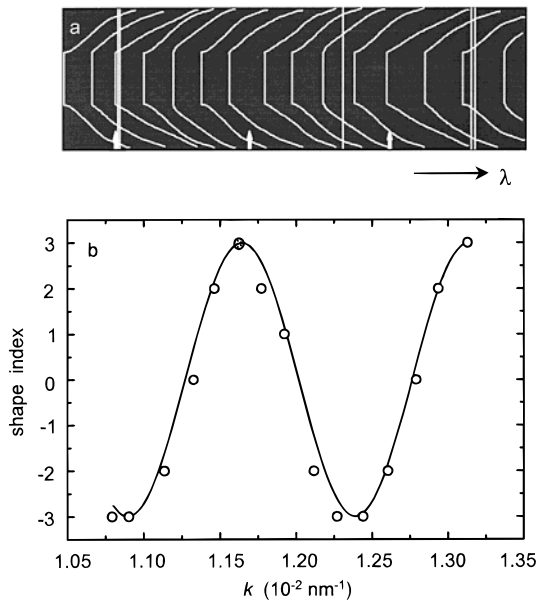

Figure 2. (a) Schematic drawing of interference fringe pattern observed for two thick, bare quartz-glass sheets in adhesive contact. Long vertical lines represent mercury spectral lines used for calibration; arrows indicate approximate wavelengths where $\cos k\Delta = 0$. (b) Shape index (see text) obtained from the fringe shapes in (a), plotted as a function of $k = 2\pi/\lambda$. The shaded data point indicates the approximate position of an inadvertently omitted wavelength measurement (the even-shaped sixth fringe from the right in (a)); this point was not included in the fit of $\cos(k\Delta + \text{constant})$ shown as a solid curve. From the fit, $\Delta = 4200$ nm.

ometer, where the relationship between the constructively interfering wavelengths and the separation between the two surfaces contains the difference in optical thickness between the substrates. Since the use of silica surfaces is of considerable interest, we will briefly illustrate the procedure for determining the separation distance developed by Horn and Smith.[31] By this method, the difference in optical thickness, Δ (typically $1-4\ \mu$m), can be deduced from the contact wavelengths of two bare sheets in adhesive contact without knowing the thickness of each sheet (typically $2-7\ \mu$m) separately.

When bare silica surfaces were brought in contact in dry air, interference fringes with different shapes could be observed as drawn in Figure 2a. The 2 nm high structures we observed with AFM (Figure 1) could not be detected due to the low resolution of about $1-2\ \mu$m in the lateral direction (the vertical direction in Figure 2a). In the case of a symmetrical interferometer, fringes arising from odd and even orders of interference have distinctly different shapes. In an asymmetric interferometer, there is an additional modulation of the fringe shapes arising from the difference in thickness, and no conclusion about odd or even order should be drawn from observing the fringe shapes alone; the order should be calculated from the contact wavelengths.

Δ can be estimated[31] from the modulation of fringe shapes by noting at least two wavelengths where a fringe of "undetermined" shape (neither "odd" nor "even") appears or two "odd" or two "even"-looking fringes next to each other (cf. arrows in Figure 2a). Since these positions are only approximately the wavelengths where $\cos k\Delta = 0$ ($k = 2\pi/\lambda$), only a rough estimate of Δ can be determined according to this procedure (described further in ref 31). An improved estimate[31] can be obtained by assigning a shape index on an arbitrary scale (from -3 to $+3$ in our example in Figure 2b) to each fringe to describe it as looking "odd" or "even". It is necessary to account for the alternating shape of odd and even fringes in the symmetrical case by multiplying every second shape index by -1. (This can be done for either the odd or the even fringes.) The resulting shape index is plotted against k, and a function of the form $\cos(k\Delta + \text{constant})$ is fitted to these data

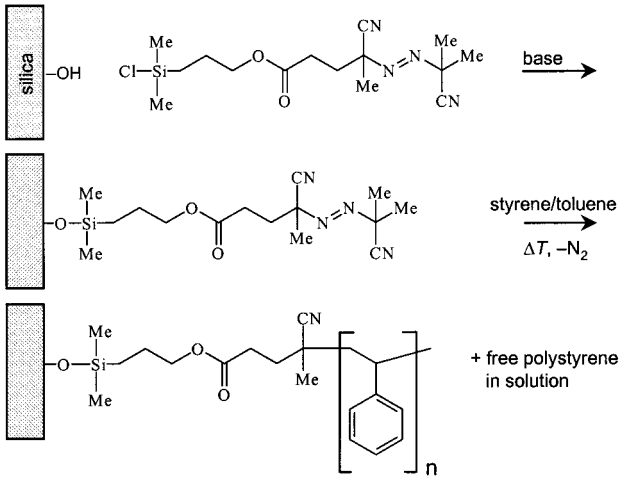

Figure 3. Reaction scheme for the grafting of the azo initiator monolayer to a silica surface and subsequent radical chain polymerization of polystyrene. Adapted from ref 27.

as shown in Figure 2b, using the rough estimate above as a starting point. A final Δ is determined by comparing distance measurements done for two different interference orders at several separations and adjusting Δ starting from the estimate above until the same distance is obtained for both fringes (taking into account the odd and even order of these fringes in the equations given in ref 31).

In this study, the zero distance ($D = 0$) between the surfaces was defined as the adhesive contact between bare quartz-glass sheets in dry air after removal of the grafted polymer at the end of the experiment, and the difference in optical thickness, Δ, was also evaluated at this point. The measurements of the dry layer thickness and of the interaction forces in toluene were thus done for a chosen fringe (order of interference) without knowing the separation distances accurately until after the experiment was finished. At the end of the experiment the brush layers in toluene were compressed with the coarser distance control of the SFA until the surfaces flattened strongly and the positions of the fringes noted as representing a separation distance below 200 nm, i.e., within one fringe separation from the contact without polymer. The surfaces were then removed from the instrument, the polymer layer was removed as described below, and the bare surfaces were remounted so that a contact position for calibration could be found as closely as possible to the one used for the force measurements.

Since the interaction forces and the preceding calibrations of movement of the surfaces were measured over a large separation distance (over 2 μm), it was convenient to use relatively thick quartz-glass sheets so that the interference fringes were closely spaced, and the same fringe could be followed in the spectrometer over the whole separation range. Since the refractive index of the quartz-glass as a function of wavelength is known[37] with much greater accuracy than for the naturally occurring mineral mica, also separation distances of several micrometers can be measured accurately when using these surfaces.

Polymer Formation. An azo initiator containing a cleavable ester group and a monochlorosilane end group was self-assembled onto the quartz-glass surfaces (attached to support disks) from a solution in dry toluene containing dry triethylamine as a catalyst (Figure 3).[25-28] The grafting reaction was allowed to proceed at room temperature overnight after which the substrates were removed and rinsed with toluene, methanol, and acetone. This procedure has been shown to result in a 1.3 ± 0.5 nm thick initiator monolayer[28] with a maximum surface coverage of approximately 1.8 μmol/m^2 or 1.1×10^{18} m^{-2} on high surface area silica gel.[25,26] The contact angle of water on the monolayers on our substrates was 67−70°. Each surface was placed in a 10 mL mixture of dry styrene and dry toluene (the volume fractions of styrene are given in Table 1),

Table 1. Description of Grafted Polystyrene Brush Layers

sample	styrene vol fraction	$M_{n,calc}$[a] (10^6 g/mol)	$M_{n,GPC}$[b] (10^6 g/mol)	M_w/M_n[b]	h_{dry} (nm)	Γ (mg/m^2)	d (nm)
A	0.5	1.4	0.9 ± 0.1	1.7	32	34	7
B	0.3	1.1	1.2 ± 0.1	1.6	20	21	10
C	0.15	0.8			16	17	8

[a] Calculated according to ref 25. [b] Determined by gel permeation chromatography.

the mixtures were degassed by three freeze−thaw cycles to remove oxygen, and the radical chain polymerization was done at 60 °C for 6 h. Subsequently, the surfaces were removed from the reaction solution, rinsed with toluene, and placed in a beaker with 100−150 mL of toluene overnight to disperse free polymer entangled in the grafted layers. The nonbonded polymer formed in the polymerization was precipitated from the reaction solution and freeze-dried for determination of the molecular weight by gel permeation chromatography (GPC) (calibrated against narrow molecular weight distribution polystyrene standards in toluene). It has been found that the M_n and M_w/M_n determined for the free polymer are similar to the values for the grafted polymer.[25,38] In one of our experiments (C in Table 1), the amount of free polymer was too small for molecular weight determination with GPC. The corresponding expected values (Table 1) were calculated from known transfer constants and the concentrations of styrene monomer and solvent.[25] The rms roughness of the dry polystyrene layers, measured with AFM over an area of $5 \times 5\ \mu m^2$, was below 1 nm,[28] and the contact angle of water was 90°. The surfaces with grafted polymer were stored under vacuum in a desiccator until measurements were done of the dry thickness, h_{dry}, of each layer from the contact between two layers in an atmosphere dried with P_2O_5 and force measurements on extended layers immersed for more than 15 h in toluene (Fisher, purity >99.9%, dried over molecular sieves and filtered through a 0.5 μm pore size Millipore Millex-SR filter).

The grafted polymer was removed from the surfaces by cleaving of the ester group in the initiator with methanol in toluene using *p*-toluenesulfonic acid as a catalyst.[25,26] After degrafting for 4 h, the remaining organic material on the surfaces was removed by photoablation (UV irradiation) with a Pen-Ray lamp (Oriel) for a total time of 1 h (in 10 min periods). Alternatively, the polystyrene layers could be removed by only UV irradiation for several hours.[25] We found that the glue layer and consequently the silver layer under the surfaces were easily affected by long UV treatments, partially due to the heating, and that the degrafting caused less damage to the silver. Control experiments showed that the contact angle of water on the surface was 68−70° after degrafting for 4 h and <8° (spreading) after 1 h of subsequent UV treatment. This suggests that a large fraction of the polystyrene is removed in the transesterification, but as expected, hydroxyl-terminated initiator fragments are still covalently attached to the surface.[25,26] These are removed, and the surface is rendered hydrophilic by the UV treatment, similarly to the bare silica surface UV treated for 1 h (cf. measurements of contact angles on silica above).

The quartz-glass surfaces glued to the support disks were found to be robust enough to withstand the temperature changes experienced (freezing in liquid N_2 and heating to 60 °C) during the grafting-from procedure. The quartz-glass sheets were glued to the supporting fused silica disks with a 1:1 mixture of dextrose and galactose, which is suitable for work in toluene at room temperature.[17] At the temperature of 60 °C used for the polymerization, the sugar mixture is not completely insoluble in toluene, but only a very small portion of the glue dissolved and neither component should be able to participate or interfere in the grafting or polymerization reactions.

Accuracy of Measurements. The roughness of the silica surfaces (0.2−0.3 nm) causes a larger error in the measurements of separation distance than when using mica surfaces, where the uncertainty is 0.1−0.2 nm.[30] In our experiments, the silica sheets were thicker than ideally chosen for measurements of small distances, and therefore the accuracy in the distance determinations was not better than 1 nm. In addition, we used a procedure (removal of the surfaces for degrafting and subsequent remounting) where the contact position might differ slightly from the one used for the measurements, so that the total uncertainty in distance is around 2 nm. The uncertainty in dry layer thickness (measured from the contact of two layers) is thus ca. 1 nm. The roughness of the dry polystyrene layers (<1 nm) contributes little to the error in average dry thickness, since the surface layer of the dry polystyrene appears to undergo flattening as two layers come into adhesive contact, as observed also in other experiments on thin polystyrene films.[18] Since the layers were fairly thick, the accuracy in the determinations of the dry layer thicknesses was thus better than 7%. If the molecular weights were known accurately, the grafting densities would then be known to 7% and the distance between grafted chains, d in Table 1, to better than 4%. However, a larger error in these parameters, likely around 30%, arises from uncertainties in the molecular weight.

In these experiments, the possible error in distance has a negligible effect on the determinations of the long-range forces, which are instead influenced by uncertainties in the measurements of the spring constant and radius, leading to a typical uncertainty of up to 10% in F/R.[29] At very large pressures (large compression), the glue supporting the quartz-glass sheets may deform, leading to an increase in radius of curvature and thus to an overestimate of F/R (where R is the radius of the undeformed contact) at the smallest separations.

Modeling of Polydisperse Brushes

Segment Density Profile. Several increasingly refined models[5−12] have been developed to describe the segment density profile of densely grafted (strongly stretched) chains in the direction normal to a substrate and the resulting range and magnitude of the interactions between two brushes or one brush and a bare surface. The earliest model for monodisperse systems proposed by Alexander[5] and de Gennes[6,7] considers a uniform segment density (i.e., a step function). This model has been applied to experimental data on monodisperse systems (for example, in refs 15−18), and its prediction of the brush height increasing linearly with the molecular weight for a fixed grafting density has been confirmed. In many cases, it also describes the pressure between two confined brushes well, especially at larger compression.

A mean field theory relaxing the assumption of a step profile has been developed by Milner et al.[8,9,12] and independently by Zhulina et al.[10,11] As in the Alexander−de Gennes model, the chain conformation is governed by the balance between osmotic pressure and elastic energy. Under conditions of strong stretching of the chains, conformational fluctuations around the most probable path may be ignored, and the "classical limit" holds.[8] An analogy between the path of a chain and the movement of a body in an external potential may be used. The "speed" then takes the role of local elongation. The speed is given by $dz/ds \propto [2(V(z) - V(z_0))]^{1/2}$ where s labels the segments along the chain, z is the spatial coordinate normal to the surface, $V(z)$ is the chemical potential in units of k_BT at z, and $V(z_0)$ is the chemical potential at the position of the free chain end z_0. For

moderate polymer concentrations, the chemical potential is proportional to the segment concentration, $V(\varphi) = w\varphi$, where w is the excluded volume. The requirement of self-consistency can be used to uniquely determine the segment density profile. For monodisperse brushes, a parabolic profile[8,9] results, as opposed to a step function used in the early papers. This refined model has also been compared to experimental force−distance curves.[9,16,18]

Even a small polydispersity results in a significantly changed segment density profile, which can also be analyzed.[9,12] Details of the calculation are given in the Appendix. Of central importance is the fact that the chain ends segregate along the brush according to chain length. The ends of the short chains are located close to the bottom, while long chains reach to the top. With the molecular weight distribution $P(n)$ as an input to the calculation, the segment density profile $\varphi(z)$ and chemical potential $V(z)$ can be determined numerically.[9,12]

Within the experimental error, the molecular weight distribution of the brushes is the same as the one of the nonattached fraction of polymer generated in the process of chain growth.[25,38] The Flory−Schulz distribution[1] usually obtained in radical chain polymerization is used in the following to describe the distribution of chain lengths inside the brush:

$$P(n) = (1 - p_r)p_r^{n-1} = \frac{M_0}{M_n}\left(1 - \frac{M_0}{M_n}\right)^{n-1} \qquad (1)$$

where $P(n)$ is the abundance of chains with n segments, $p_r \lesssim 1$ the probability that a monomer has reacted, M_0 the monomer weight ($M_0 = 104$ g/mol for polystyrene), and M_n the number-averaged molecular weight (in our case, the values determined by GPC for samples A and B and an estimated value for sample C). For computational purposes the distribution was cut off at the high end at $n_{cut} = 10M_n/M_0$.

The parameters needed to map this theory onto the experiment are the thermal energy k_BT, the statistical segment length b, and the excluded volume w. For polystyrene in toluene, $b = 0.76$ nm is calculated from the end-to-end distance given in ref 39. The parameter v occurring in the Edwards Hamiltonian in refs 8 and 9 is equal to $3/b^2$. With regard to the excluded-volume parameter of polystyrene in toluene, a range of w from $(0.20\text{ nm})^3$ to $(0.23\text{ nm})^3$ is obtained from second virial coefficients based on light scattering experiments, tabulated in ref 39. A larger value of $w = (0.32\text{ nm})^3$ can be found in the literature on osmotic pressure measurements.[40,41] It will be shown below that the model predictions depend rather sensitively on the choice of the excluded-volume parameter.

Figure 4a shows the assumed Flory−Schulz molecular weight distribution for $M_n = 0.9 \times 10^6$ and 1.2×10^6 g/mol from GPC measurements (samples A and B) and an estimated $M_n = 0.7 \times 10^6$ g/mol for sample C. (This value was not obtained from GPC measurements but estimated from the polymerization conditions. It will be seen below that this estimate, well within the typical deviations of the measured values from the expected as given in Table 1, gave a similar agreement with the experimental force curve for sample C as the GPC values gave for samples A and B, and it was thus used for all calculations in the following.) The molecular weight distribution is rather broad ($M_w/M_n \sim 2$). If, as

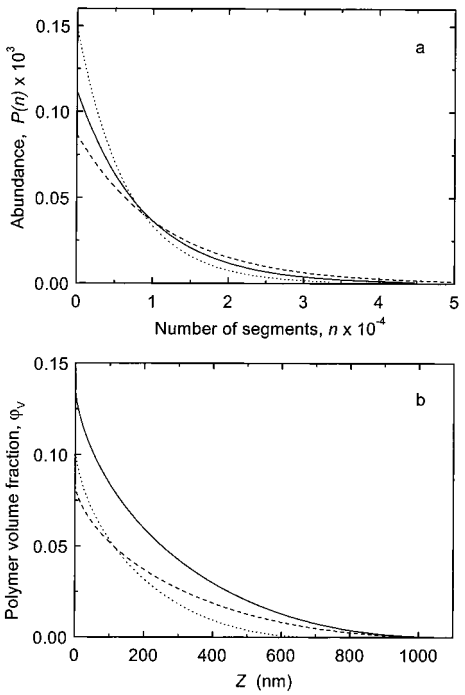

Figure 4. (a) Flory−Schulz molecular weight distribution used as an input to the modeling. Solid curve: sample A, $M_n = 0.9 \times 10^6$ g/mol. Dashed curve: sample B, $M_n = 1.2 \times 10^6$ g/mol. Dotted curve: sample C, $M_n = 0.7 \times 10^6$ g/mol. (b) Segment density profiles for the uncompressed brush layers resulting from the distributions in (a) with $w = (0.23\text{ nm})^3$ and grafting densities of 2.2×10^{16}, 1.0×10^{16}, and 1.4×10^{16} chains/m^2. The distributions are almost exponential.

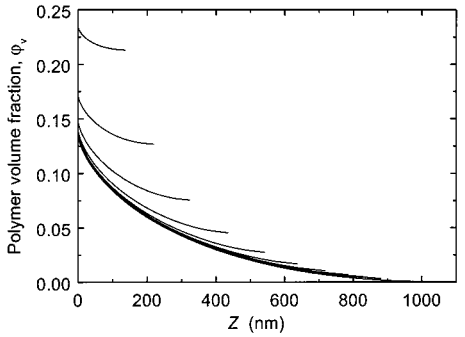

Figure 5. Calculated segment density profiles under compression for sample A with $w = (0.23\text{ nm})^3$.

stated in ref 9, even small polydispersities of $M_w/M_n = 1.02$ affect the brush height by as much as 10%, a large polydispersity will certainly have a very profound effect. The segment density profiles derived for the molecular weights above and $w = (0.23\text{ nm})^3$ are shown in Figure 4b. Clearly, the profiles do not resemble the parabolic profiles found for monodisperse brushes.

During compression the external pressure p enters the calculation. The chemical potential at the outer edge of the brush is not zero but is instead given by $V(h) = (2wp)^{1/2}$. The calculation in this case becomes more complicated but not fundamentally different from the approach described above. The brush height h is now a function of the applied pressure p. Figure 5 shows the segment density profile for sample A and $w = (0.23\text{ nm})^3$ under various external pressures. As the gap between the cylinders becomes more narrow, the segment density increases and the profile flattens out.

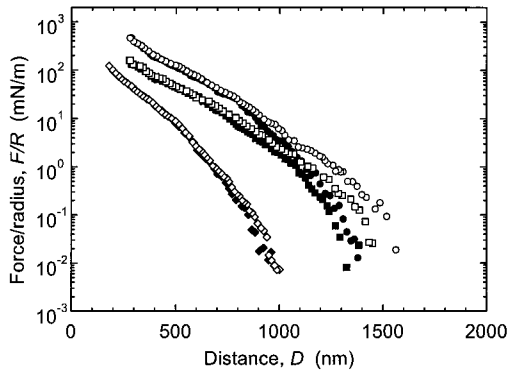

Figure 6. Experimentally determined interaction force F (normalized by the radius of curvature of the undeformed surfaces, R) as a function of distance, D, measured between two surfaces covered with strongly stretched polystyrene brushes in toluene at 25 °C. $D = 0$ is the contact between bare quartz-glass surfaces in the absence of polymer. Open symbols denote approach (compression) and filled symbols separation (decompression) of sample A (○, ●), B (□, ■), and C (◇, ◆). The thickness of two polystyrene layers in contact without solvent was 65, 41, and 32 nm, respectively, giving the dry layer thickness on one surface, h_{dry}, in Table 1.

Results and Discussion

Forces on Compression. The forces measured between two surfaces covered with polystyrene brushes (samples A−C in Table 1) in toluene at 25 °C (good solvent conditions) were repulsive over the whole interaction range (Figure 6). The repulsion observed on approach started at $D \geq 1\ \mu$m in all three systems, and in each case, a slightly lower magnitude and range of the force were measured on separation (most apparent for the higher molecular weight systems A and B). Because of the long range, which has also been observed in other studies[32−34] on similar systems, the time required to measure one approach and separation of the surfaces (compression and decompression) with the sensitive motor control was 45 min−1 h. Control experiments showed no difference in the interaction range and magnitude on approach and separation compared to the results in Figure 6 if the measurements were done more slowly over ca. 2 h.

The theoretically predicted force between two crossed cylinders, normalized by the radius of curvature, was derived from the free energy of two flat plates using the Derjaguin approximation.[35]

$$\frac{F(D)}{R} = 2\pi W(D) \qquad (2)$$

where eq A10 from the Appendix was used to calculate the free energy $W(D)$.

In Figure 7 the force vs distance curves corresponding to segment density profiles of the type shown in Figure 5 are superimposed on the experimental data on compression (from Figure 6). The statistical segment length $b = 0.76$ nm was kept fixed. As specified in the figure caption, the molecular weights measured by GPC were used for samples A and B. A molecular weight of 0.7×10^6 g/mol was chosen for sample C, as described in the Modeling section. The choice of molecular weight has a strong influence on the calculated brush height but much less influence on the slope of the force−distance curve. The excluded volume w, on the other hand, affects both the slope and the extension of the interaction. The boundaries of w obtained from light scattering[39] and

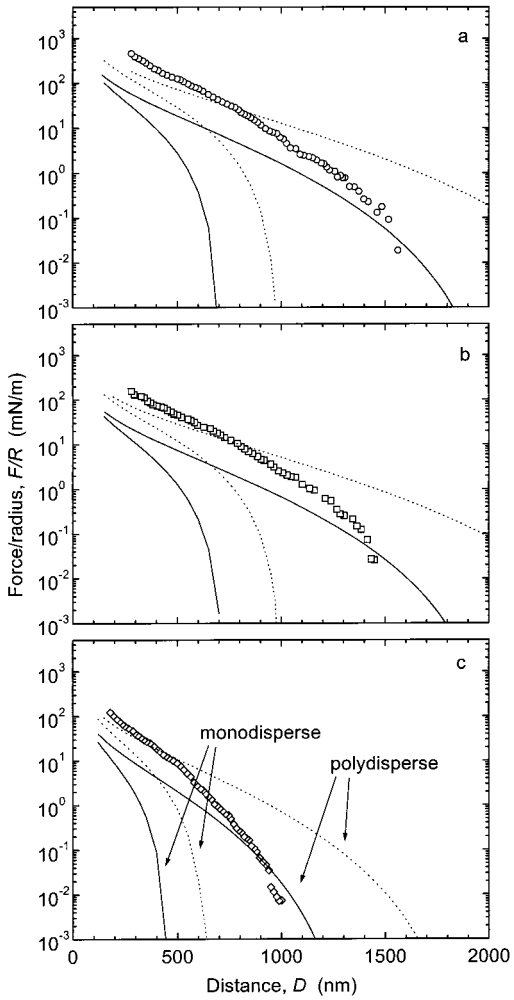

Figure 7. Comparison between measured interaction forces (open symbols, as in Figure 6) and theoretically predicted (curves) on compression of two surfaces covered with (a) sample A, $M_n = 0.9 \times 10^6$ g/mol, grafting density 2.2×10^{16} m^{-2}; (b) sample B, $M_n = 1.2 \times 10^6$ g/mol, grafting density 1.0×10^{16} m^{-2}; and (c) sample C, $M_n = 0.7 \times 10^6$ g/mol, grafting density 1.4×10^{16} m^{-2}. In each panel, the two curves on the left were calculated for a monodisperse brush,[8,9] and the two curves extending to the right were calculated for the polydisperse[8,12] molecular weight distributions in Figure 4a as described in the text. Solid curves indicate $w = (0.23\ \text{nm})^3$ and dotted curves $w = (0.32\ \text{nm})^3$.

osmotic pressure measurements,[40,41] $(0.23\ \text{nm})^3$ and $(0.32\ \text{nm})^3$, respectively, were used as indicated in the figure caption. Our experimental data lie between the theoretical curves obtained for these values. Independent information from ellipsometry measurements[33,42] of the swollen thickness of dense, high molecular weight polystyrene brushes in toluene, formed by the same grafting-from procedure as our systems, suggests a w of about $(0.27\ \text{nm})^3$.

As expected, calculations for monodisperse brushes[9] (the two curves on the left in each panel in Figure 7) do not describe our systems. At large compression, the prediction for the polydisperse system merges with the one for the monodisperse, since in this limit, the interactions are dominated by osmotic pressure. However, at larger compression (small D), the measured forces exceed the theoretical ones. It is known that at large pressures the glue supporting the surfaces can deform so that the radius of curvature increases.[43] Since the measured forces were normalized by the radius of

curvature of the undeformed surfaces, such a deformation would result in an apparent increase in our experimentally determined F/R. The deformation as a function of load has been investigated for mica glued with epoxy glue,[43] but not for silica sheets and the sugar mixture we used. From the mica data, we estimate that at $F/R \approx 100$ mN/m in our figures the value of R used might be too small by a factor 2−3, which might account for part of the discrepancy between the experimental F/R and the theory at this high load. However, upon closer inspection, the slopes of the experimental force curves are different from the theoretical throughout the whole distance range. Potentially, three-body interactions are the cause of these discrepancies.[44] For an order of magnitude estimation we write the chemical potential including three-body interactions as $V(\varphi) = (w/V_{mon})\varphi_V + (u/V_{mon})^2\varphi_V^2$, where φ_V is the polymer volume fraction, V_{mon} the monomer volume, and u a three-body excluded volume. As a first-order approximation one may assume $u \approx V_{mon}$.[45] Three-body interactions become appreciable when the two terms entering the chemical potential are of equal magnitude, that is, at $\varphi_{V,c} \approx w/V_{mon} = 0.07$, where $w = (0.23\ \text{nm})^3$ and $V_{mon} = (0.55\ \text{nm})^3$ were used. This polymer volume fraction is within the range of concentrations encountered in the brushes. Interestingly, an increase of force with compression steeper than the predictions from self-consistent field theory was also found in a molecular dynamics study on monodisperse brushes,[46] where it was concluded that the deviations were caused by a monomer density above the semidilute regime.

Entanglement Effects. The brushes investigated here differ from previously used systems not only because of their polydispersity but also by the combination of high density and high molecular weight. Specifically, the chain length may exceed the entanglement length. Since entanglements should affect the dynamic behavior, we searched for relaxation effects related to chain disentanglement. We are concerned with entanglements *within one single brush layer*, not entanglements between the brushes on the two opposed surfaces. The latter kind of entanglements should still be small due to the large chain stretching.[46] We never observed adhesion that could indicate interbrush entanglements.

It was not practical to let the approach and separation take many hours, since thermal drift might occur. Instead, the approach was done at a similar rate as in Figure 6, and at the smallest separation ($D \approx 200-250$ nm), the brush layers were left compressed for 1 h. On separation, again at a rate similar to the measurements in Figure 6, we observed a decrease in the magnitude and range of the force (Figure 8a). This effect was most pronounced for samples A and B. When a new approach of the surfaces was done directly after these measurements (in practice ca. 30 min later, since it was necessary to separate the surfaces to $D > 2\ \mu$m to do calibrations of the motor movement on separation and on the new approach), the range of the interaction (i.e., the extension of the polymer brush) was found to be shorter, and the difference between the force curves on approach and separation was considerably smaller (Figure 8b). The range now coincided with the range observed on separation in the previous measurement (shown as filled symbols in Figure 8a). Several subsequent approach and separation measurements after different waiting times showed that the extension and the original, rather small difference between approach and separation recovered with time: After 6 h (Figure 8c), the interaction range and relaxation effects were similar to the ones in Figure 6, regardless of whether the surfaces had been left separated for 6 h or if several measurements (without long compression times) had been taken during that time. Relaxation effects were only observed after the samples had remained in the compressed state over extended times. The magnitude of the force observed at small separations (strong compression), which is expected to be of osmotic origin and thus only concentration dependent, was not affected by the compression time.

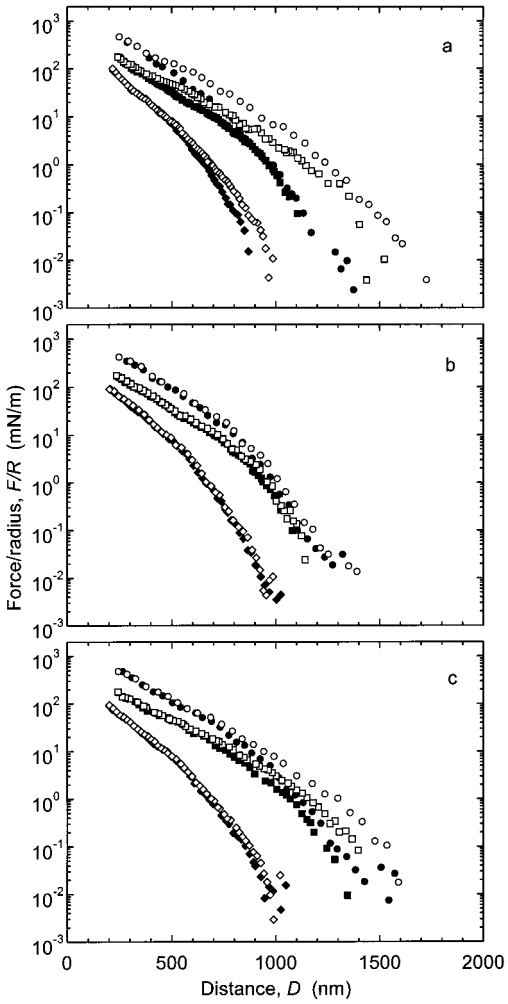

Figure 8. Interaction forces between the polymer brush layers specified in Figure 6 as a function of distance. Symbols as in Figure 6. (a) Changes in magnitude and range of the force after long compression: The approach (open symbols) was done as in Figure 6; then the surfaces were left at the largest compression for each sample ($D \approx 200-250$ nm) for 1 h and then separated (filled symbols) at the same rate as in Figure 6. (b) Subsequent compression started within 30 min of finishing the measurements in (a), showing shorter ranges of interactions and smaller difference between approach and separation. The force curves correspond closely to the ones obtained on separation in (a). (c) Forces measured after the brush layers had relaxed for 6 h: The interaction range and difference between the curves on approach and separation seen in Figure 6 were recovered.

We attribute the differences in the force curves after long compression times to stress relaxation caused by chain disentanglements inside the brush layers. Entanglement between the two brushes should be prevented by the chain stretching.[46,47] To our knowledge, entanglement effects *inside* brushes have not been

discussed because in previous studies, the brushes did not reach the thicknesses where entanglement effects appear. Brushes grown by the grafting-from technique may, however, be substantially entangled. The samples investigated here showed some entanglement, and much thicker samples can be synthesized.

In the following, we substantiate this argument by estimating a "typical disentanglement time". Naturally, the distribution of disentanglement times is at least as broad as the molecular weight distribution, since the time depends on the chain length and on the distance from the surface. For instance, entanglements formed by long chains near the solid surface would be the most long-lived, and likely their disentanglement time would exceed the "typical" time calculated below by orders of magnitude. Given this limitation, we have confined ourselves to simple arguments with limited quantitative accuracy. We draw on the analogy between a brush and a star polymer. Stress relaxation in star polymers has been considered in substantial depth,[48] and the resulting picture can be transferred to the brush case.

To estimate the time scale for stress relaxation, we calculate the frequency with which a typical chain retracts down to the bottom of the brush, such that it escapes all topological constrains. A "typical" chain could, for instance, be a chain with a length n equal to the average length $n_{ave} = M_n/M_0$. We view chain retraction as an activated process, where the attempt frequency is the inverse Rouse time and the activation energy has two contributions: the energy associated with the contour length fluctuation of the primitive path, U_{CLF}, and the osmotic energy U_{osm} required to move the chain down to the crowded bottom of the brush. The estimated disentanglement time is

$$\tau_d \approx \tau_R \exp\left(\frac{U_{CLF} + U_{osm}}{k_B T}\right) \qquad (3)$$

The most simple model to account for contour length fluctuations treats the chain as an entropic spring. It yields $U_{CLF} = 3k_BTL^2/(2nb^2)$ (eq 16 in ref 48) with L the length of the primitive path. However, this equation substantially underestimates the rates of stress relaxation found in experiments on star polymers. Ball and McLeish[49] have proposed an alternative expression which accounts for the fact that the tube widens as the chain retracts. Although more sophisticated expressions have been derived later,[50] we use the model from ref 49 for simplicity. According to this model,

$$U_{CLF} = \frac{15}{24} k_B T \frac{M_n}{M_e} \qquad (4)$$

with M_e the entanglement molecular weight. The factor M_n/M_e counts the number of entanglements. We have set the parameter s from eq 22 in ref 48 equal to the length of the primitive path L; i.e., we calculate the energy required to completely retract the chain from its original tube. The entanglement molecular weight M_e depends on concentration. For polystyrene melts ($\varphi = 1$) it was determined from the plateau modulus G_0 as $M_{e,melt} \sim 18\,000$ g/mol.[51−53] Upon dilution, the entanglement molecular weight increases as $M_e \sim \varphi^{-\alpha}$ with α an exponent between 1 and 1.15.[51,54,55] We have used $\alpha = 1$ for simplicity. For the calculation of the effective entanglement length we used $M_{e,eff} = M_{e,melt}\langle\varphi^{-1}\rangle$, where the angular brackets denote the average over the entire chain. For our uncompressed brushes the number of entanglements is approximately 3−5.

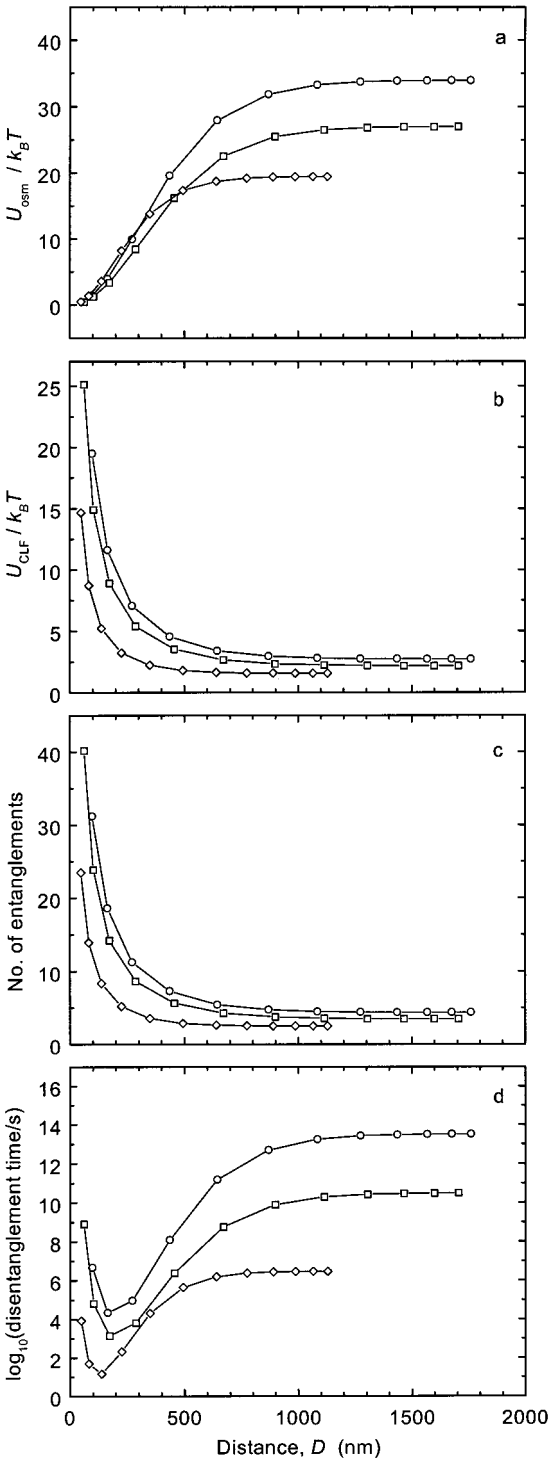

Figure 9. Estimation of disentanglement times for a chain with the average chain length M_n/M_0: (a) entropic penalty for chain retraction caused by osmotic pressure, U_{osm}; (b) entropic penalty for chain retraction associated with the contour length fluctuation, U_{CLF}; (c) number of entanglements; and (d) disentanglement time. Results are shown for $w = (0.23\ \text{nm})^3$ and sample A (○), B (□), and C (◇). The osmotic term dominates the disentanglement time at large separations. It becomes less important at higher compression, but in this case the narrowing tube width again slows down the disentanglement.

The second contribution to the activation energy arises from the fact that the chemical potential is higher

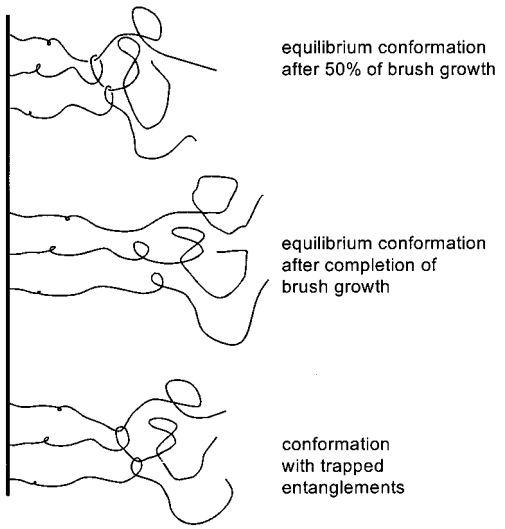

Figure 10. Illustration of the effects of entanglements on thick brushes. In very thick brushes (dry thickness $h_{dry} > 30$ nm) some entanglements formed during brush growth are never released. These persisting topological constraints exert a compressive force onto the brush.

at the foot of the brush than at the tail. This energy is obtained in the calculations of the force−distance curves as the integral of the chemical potential over the chain. We approximate the osmotic part of the activation energy by the difference between the equilibrium energy and the energy in a conformation where the chain is entirely located at the foot of the brush.

The attempt frequency is given by the inverse Rouse time[56] $\tau_R^{-1} = [\zeta_0 n^2 b^2/(3\pi^2 k_B T)]^{-1}$, where ζ_0 is the monomeric friction coefficient. We have used the value $\zeta_0 = 6\pi\eta R_{mon} = 10^{-11}$ N s m^{-1} with the viscosity $\eta \sim 10^{-3}$ Pa s and the monomer radius $R_{mon} \sim 0.5$ nm. This roughly agrees with what one gets if one uses the tabulated values[57] of ζ_0 at T_g and accounts for the effect of dilution with the shift factors from ref 53.

The outcome of this calculation is summarized in Figure 9 for $w = (0.23\text{ nm})^3$. (For clarity, the data for $w = (0.32\text{ nm})^3$ are not shown.) The osmotic term dominates the disentanglement time at large separations. The osmotic penalty becomes less important at higher compression, but in this regime the narrowing tube width slows down the disentanglement. At the separation $D = 200-250$ nm, where the brushes were kept compressed for 1 h (cf. Figure 8a), the estimated disentanglement time (Figure 9d) is minutes to hours for all choices of parameters, including $w = (0.32\text{ nm})^3$. We again emphasize that the calculation only yields an order of magnitude. Given the estimated disentanglement times above, we find it plausible to attribute the relaxation observed in the experiment to entanglement effects.

Finally, we note that the brushes investigated here were not particularly thick. Brushes with a dry thickness in the range of 1 μm have been produced from poly(methyl methacrylate),[38] and in a solvent they swell to a thickness of several micrometers. Our calculation shows that the time needed for even modest disentanglement becomes very large, which implies that such thick brushes can never reach equilibrium. This situation is schematically depicted in Figure 10.

During the polymerization, the grafting density of the chains gradually increases. When the brush has grown to an equivalent dry thickness of about 30 nm, the entanglements start to be trapped. These topological constraints remember the equilibrium chain conformation at the instant they were formed. In the early stages of brush growth the individual chains are random coils, and entanglements form between chains that are about a radius of gyration apart. As more chains grow, chain crowding increases the osmotic pressure and the chains stretch. However, the entanglements impede the chain stretching toward the equilibrium conformation and exert a pressure in addition to elastic pressure caused by stretching. Eventually the brush thickness will be less than the equilibrium value because the chains have spread out sideways to satisfy the topological constraints. The entanglements should also affect the osmotic pressure inside a brush, which could possibly be measured by growing the brush on a flexible substrate and measuring its deflection.

Conclusion

We have measured the repulsive force between high molecular weight polystyrene brushes attached to silica surfaces by a grafting-from technique. The measured force as a function of separation distance agrees reasonably well with self-consistent-field predictions for polydisperse brushes in a good solvent. The slightly larger slopes of the force−distance curves obtained in the experiments are attributed to a segment density in the brush above the semidilute regime. When leaving the brush layers in a compressed state for 1 h, they relax and show substantially decreased repulsive forces on separation. The original force−distance curves are recovered after several hours. We attribute these slow relaxations to chain disentanglements inside the brushes.

Acknowledgment. We thank R. Horn and D. Antelmi for very helpful discussions on the distance calculations for an asymmetrical interferometer. I. Kärcher, M. Knecht, and our glassblower, A. Egenolf, are thanked for technical assistance and V. Scheumann for performing the AFM measurements. Discussions with O. Prucker, P. Schorr, and S. Milner are gratefully acknowledged. M.R. thanks the Alexander von Humboldt Foundation for a research fellowship.

Appendix. Details of the Calculation of the Segment Density Profiles and the Force−Distance Curves

The calculation of segment density profiles closely followed the procedures outlined in ref 12. For completeness, we briefly repeat the formalism. Both energy and length are dimensionless: the unit energy is the thermal energy $k_B T$, and the unit length is $3^{-1/2}b$ where b is the statistical segment length. The unit length is equal to $v^{-1/2}$ with v the parameter from the Edwards Hamiltonian in ref 9. In ref 12 the excluded volume w is dimensionless. Since the unit volume is already uniquely defined by the statistical segment length, b, the difference between the excluded volume w and the unit volume has to be accounted for by "counting" the segments in a somewhat unusual way. The segment concentration is redefined in such a way that the chemical potential $V(\varphi)$ is given by $V(\varphi) = \varphi = (3^{3/2}w/b^3)\varphi^*$. Here, the quantity φ^* is the number of segments per unit volume, and the prefactor $3^{3/2}w/b^3$ is the excluded volume divided by the unit volume $3^{-3/2}b^3$. The same redefinition of concentration applies to the grafting density; that is, the grafting density σ from ref 12

is replaced by the quantity $(3^{3/2}w/b^3)\sigma^*$, where σ^* is the number of chains per unit area. The coverage σ^* is calculated from the dry thickness and the molecular weight as

$$\sigma^* = \frac{h_{\mathrm{dry}}\rho N_{\mathrm{A}}}{M_{\mathrm{n}}}\frac{b^2}{3} \tag{A1}$$

where h_{dry} is the dry thickness, ρ the density, N_{A} Avogadro's number, and M_{n} the number-averaged molecular weight. Note that both σ^* and φ^* are still dimensionless. However, the "counting" of segments occurs in the conventional way which implies that the excluded volume is not identical to the unit volume. The chemical potential at the bottom of the brush in units of $k_{\mathrm{B}}T$, A, is given by

$$A = \frac{3}{2}\left(\frac{\pi^2}{12}\right)^{1/3}\left(\frac{3^{3/2}w}{b^3}\sigma^*\right)^{2/3} \tag{A2}$$

In the following the "potential energy" $U(z) = A - V(z)$ is used as the independent variable instead of z. Because the chain ends segregate along the brush, there is a one-to-one correspondence between the location of the ends of the chains of length n, $z_0(n)$, and the potential energy $U(z_0(n))$. The spatial variable z can be eliminated. $U(n)$ is given by

$$U(n) = A\left[1 - \left(1 - \frac{\sigma^*(n)}{\sigma^*}\right)^{2/3}\right] \tag{A3}$$

where $\sigma^*(n)$ is the number of chains per unit area with a chain length less than or equal to n. For the Flory–Schulz distribution one has

$$\sigma^*(n) = \sigma^*\int_0^n P(n')\,\mathrm{d}n' = \sigma^*\int_0^n (1-p_{\mathrm{r}})p_{\mathrm{r}}^{\,n'-1}\,\mathrm{d}n' = \sigma^*\frac{1-p_{\mathrm{r}}}{p_{\mathrm{r}}\ln(p_{\mathrm{r}})}(p_{\mathrm{r}}^{\,n}-1) \tag{A4}$$

with $p_{\mathrm{r}} \lesssim 1$ the probability that any given monomer has reacted. $(1 - p_{\mathrm{r}})^{-1}$ is equal to the number-averaged chain length M_{n}/M_0.

Since $U(n)$ (determined with eq A3) is a monotonic function, it can be numerically inverted to yield the function $n(U)$. The derivative of z with respect to U is given by

$$\frac{\mathrm{d}z}{\mathrm{d}U}(U) = \frac{\sqrt{2}}{\pi}\int_0^{n(U)}\frac{1}{\sqrt{U-U(n)}}\,\mathrm{d}n \tag{A5}$$

The function $z(U)$ follows from eq A5 by integration. Since $z(U)$ is monotonic, it can be inverted to give $U(z)$. The number of segments per unit volume $\varphi^*(U)$ follows from the definition of the chemical potential V as

$$\varphi^*(V(z)) = \frac{b^3}{3^{3/2}w}V(z) = \frac{b^3}{3^{3/2}w}(A - U(z)) \tag{A6}$$

The polymer volume fraction shown in Figures 4b and 5 is given by

$$\varphi_{\mathrm{V}} = \varphi^*\frac{M_0}{\rho}\frac{3^{3/2}}{b^3} \tag{A7}$$

The physical distance from the substrate Z is related to the dimensionless coordinate z by

$$Z = \frac{b}{\sqrt{3}}z \tag{A8}$$

When an external pressure p compresses the brush, the segment concentration at the outer edge $z = h$ is no longer zero. The osmotic pressure at the outer edge is $p = {}^1/_2\varphi^2$. This affects the potential energy. One arrives at

$$\frac{3^{3/2}w}{b^3}(\sigma^* - \sigma^*(n)) = \frac{2^{5/2}}{3\pi}\left[(A(p) - U(n;p))^{3/2} + \frac{3p^{1/2}}{2^{1/2}}(A(p) - U(n;p))^{1/2}\right] \tag{A9}$$

which is a cubic equation in $(A(p)-U(n;p))^{1/2}$. $A(p)$ is obtained by setting $n = 0$. With $U(n;p)$ given from the solution of eq A9, the segment concentration is calculated with eqs A5–A7 as before.

We calculate the energy of compression as the integral over $p\mathrm{d}h(p)$, with $\mathrm{d}h(p)$ the increment in brush height $h(p)$. However, care has to be taken with regards to the units of p. In ref 12 the pressure is defined as $p = {}^1/_2\varphi^2$, where the density φ has been defined such that $w \equiv 1$. We define a pressure p^* equal to $p/(3^{3/2}w/b^3)$. With this prefactor, one has $p^* = {}^1/_2(3^{3/2}w/b^3)\varphi^{*2}$, and the pressure p^* has the dimensions of $k_{\mathrm{B}}T$ per unit volume. The energy of compression of two brushes in SI units is then

$$W(h) = 2\frac{k_{\mathrm{B}}T}{3^{-3/2}b^3}\int_{h(p=0)}^{h(p)} p^*(h)\,\mathrm{d}h \tag{A10}$$

where the factor of 2 accounts for the presence of two brushes. Finally, the force normalized by the radius of curvature, $F(D)/R$, as a function of the separation $D = 2h$ is given by the Derjaguin approximation as

$$\frac{F(D)}{R} = 2\pi W(D) \tag{A11}$$

which completes the calculation.

References and Notes

(1) See, for example: Young, R. J.; Lovell, P. A. *Introduction to Polymers*, 2nd ed.; Chapman & Hall: London, 1991.
(2) Berman, A.; Steinberg, S.; Campbell, S.; Ulman, A.; Israelachvili, J. N. *Tribol. Lett.* **1998**, *4*, 43.
(3) Dijt, J. C.; Cohen Stuart, M. A.; Fleer, G. J. *Macromolecules* **1994**, *27*, 3207.
(4) Dolan, A. K.; Edwards, S. F. *Proc. R. Soc. London A* **1974**, *337*, 509.
(5) Alexander, S. *J. Phys. (Paris)* **1977**, *38*, 983.
(6) de Gennes, P. G. *Macromolecules* **1980**, *13*, 1069.
(7) de Gennes, P. G. *Adv. Colloid Interface Sci.* **1987**, *27*, 189.
(8) Milner, S. T.; Witten, T. A.; Cates, M. E. *Macromolecules* **1988**, *21*, 2610.
(9) Milner, S. T. *Europhys. Lett.* **1988**, *7*, 695.
(10) Zhulina, E. B.; Borisov, O. V.; Priamitsyn, V. A. *J. Colloid Interface Sci.* **1990**, *137*, 495.
(11) Zhulina, E. B.; Borisov, O. V.; Pryamitsyn, V. A.; Birshtein, T. M. *Macromolecules* **1991**, *24*, 140.
(12) Milner, S. T.; Witten, T. A.; Cates, M. E. *Macromolecules* **1989**, *22*, 853.
(13) Chen, Y.-L.; Helm, C. A.; Israelachvili, J. N. *J. Phys. Chem.* **1991**, *95*, 10736.
(14) Peanasky, J.; Schneider, H. M.; Granick, S.; Kessel, C. R. *Langmuir* **1995**, *11*, 953.

(15) Kuhl, T. L.; Leckband, D. E.; Lasic, D. D.; Israelachvili, J. N. In *Stealth Liposomes*; Lasic, D., Martin, F., Eds.; CRC Press: Boca Raton, 1995; pp 73−91.
(16) Taunton, H. J.; Toprakcioglu, C.; Fetters, L. J.; Klein, J. *Macromolecules* **1990**, *23*, 571.
(17) Hadziioannou, G.; Patel, S.; Granick, S.; Tirrell, M. *J. Am. Chem. Soc.* **1986**, *108*, 2869.
(18) Watanabe, H.; Tirrell, M. *Macromolecules* **1993**, *26*, 6455.
(19) Watanabe, H.; Matsuyama, S.; Mizutani, Y.; Kotaka, T. *Macromolecules* **1995**, *28*, 6454.
(20) Vigil, G.; Xu, Z.; Steinberg, S.; Israelachvili, J. *J. Colloid Interface Sci.* **1994**, *165*, 367.
(21) Horn, R. G.; Smith, D. T.; Haller, W. *Chem. Phys. Lett.* **1989**, *162*, 404.
(22) Horn, R. G.; Smith, D. T. *J. Non-Cryst. Solids* **1990**, *120*, 72.
(23) Grabbe, A.; Horn, R. G. *J. Colloid Interface Sci.* **1993**, *157*, 375.
(24) Grabbe, A. *Langmuir* **1993**, *9*, 797.
(25) Prucker, O. Ph.D. Thesis, University of Bayreuth, Germany, 1995.
(26) Prucker, O.; Rühe, J. *Macromolecules* **1998**, *31*, 592.
(27) Prucker, O.; Rühe, J. *Macromolecules* **1998**, *31*, 602.
(28) Prucker, O.; Rühe, J. *Langmuir* **1998**, *14*, 6893.
(29) Israelachvili, J. N.; Adams, G. E. *J. Chem. Soc., Faraday Trans. 1* **1978**, *74*, 975.
(30) Israelachvili, J. N. *J. Colloid Interface Sci.* **1973**, *44*, 259.
(31) Horn, R. G.; Smith, D. T. *Appl. Opt.* **1991**, *30*, 59.
(32) Domack, A.; Prucker, O.; Rühe, J.; Johannsmann, D. *Phys. Rev. E* **1997**, *56*, 680.
(33) Habicht, J.; Schmidt, M.; Rühe, J.; Johannsmann, D. *Langmuir* **1999**, *15*, 2460.
(34) Butt, H. J.; Kappl, M.; Mueller, H.; Raiteri, R.; Meyer, W.; Rühe, J. *Langmuir* **1999**, *15*, 2559.
(35) Derjaguin, B. V. *Kolloid Z.* **1934**, *69*, 155.
(36) Iler, R. K. *The Chemistry of Silica*; Wiley: New York, 1979.
(37) Product information, Heraeus Quarzglas GmbH, Hanau, Germany, 1994.
(38) Schimmel, M. Ph.D. Thesis, University of Mainz, Germany, 1998.
(39) *Polymer Handbook*, 3rd ed.; Brandrup, J., Immergut, E. H., Eds.; Wiley: New York, 1989.
(40) Schick, M. J.; Doty, P.; Zimm, B. H. *J. Am. Chem. Soc.* **1950**, *72*, 530.
(41) Kuwahara, N.; Okazawa, T.; Kaneko, M. *J. Chem. Phys.* **1967**, *47*, 3357.
(42) Habicht, J. Ph.D. Thesis, University of Mainz, Germany, 1998.
(43) Horn, R. G.; Israelachvili, J. N.; Pribac, F. *J. Colloid Interface Sci.* **1987**, *115*, 480.
(44) Anderson, P.; Hong, D. C.; Lam, P. M.; Vugmeister, B. E. *J. Phys. II (Paris)* **1994**, *4*, 1157.
(45) Fleer, G. J.; Cohen Stuart, M. A.; Scheutjens, J. M. H. M.; Cosgrove, T.; Vincent, B. *Polymers at Interfaces*; Chapman and Hall: London, 1993; p 6.
(46) Murat, M.; Grest, G. S. *Phys. Rev. Lett.* **1989**, *63*, 1074.
(47) Klein, J.; Kumacheva, E.; Perahia, D.; Mahalu, D.; Warburg, S. *Faraday Discuss.* **1994**, *98*, 173.
(48) McLeish, T. C. B.; Milner, S. T. *Adv. Polym. Sci.* **1999**, *143*, 195.
(49) Ball, R. C.; McLeish, T. C. B. *Macromolecules* **1989**, *22*, 1911.
(50) Milner, S. T.; McLeish, T. C. B. *Macromolecules* **1997**, *30*, 2159; see also Figure 7 in ref 48.
(51) Ferry, J. D. *Viscoelastic Properties of Polymers*; Wiley: New York, 1980.
(52) Onogi, S.; Masuda, T.; Kitagawa, K. *Macromolecules* **1970**, *3*, 109.
(53) Plazek, D. J.; Riande, E.; Markovitz, H.; Raghupathi, N. *J. Polym. Sci., Polym. Phys.* **1979**, *17*, 2189.
(54) Isono, Y.; Fujimoto, T.; Takeno, N.; Kjiura, H.; Nagasawa, M. *Macromolecules* **1978**, *11*, 888.
(55) Graessley, W. W. *Adv. Polym. Sci.* **1974**, *16*, 1.
(56) See, for example: Doi, M.; Edwards, S. F. *The Theory of Polymer Dynamics*; Clarendon Press: Oxford, 1986; p 196.
(57) Reference 51, p 330.

MA9920994